Articles

Prediction of the Coordination Scheme of Lanthanide N-Tetrasubstituted Tetraazamacrocycles: An X-ray Crystallography and Molecular Modeling Study

Claude Lecomte,*,† Valérie Dahaoui-Gindrey,† Hervé Chollet,‡,§ Claude Gros,‡ Anil K. Mishra,‡ Frédéric Barbette,‡ Pluton Pullumbi,‡ and Roger Guilard*,‡

Laboratoire de Cristallographie et Modélisation des Matériaux Minéraux et Biologiques (LCM^{3}B), URA CNRS No. 809, Université Henri Poincaré, Nancy 1, Faculté des Sciences, B.P. 239, 54506 Vandoeuvre lès Nancy CEDEX, France, and Laboratoire d'Ingénierie Moléculaire pour la Séparation et les Applications des Gaz (LIMSAG), UMR No. 5633, Université de Bourgogne, Faculté des Sciences Gabriel, 6 Bd Gabriel, 21000 Dijon, France

Received August 2, 1996[⊗]

The synthesis and characterization of three lanthanide (Ce, Gd, Eu) complexes with the 1,4,8,11-tetrakis-(2-carboxyethyl)-1,4,8,11-tetraazacyclotetradecane ligand (TETP) are described. Crystal structures of $[Ce(H_2TETP)](OH)(H_2O)\cdot 10H_2O$ (**1**), $[Gd(H_3TETP)](OH)_2(H_2O)_2\cdot 3H_2O$ (**2**), and $[Eu(H_3TETP)](OH)_2(H_2O)_2\cdot 3H_2O$ (**3**) are reported. Crystal data: (**1**) monoclinic, *C*2/*c*, $a = 29.523(4)$ Å, $b = 17.492(3)$ Å, $c = 8.509(1)$ Å, $\beta = 98.72(1)°$, $V = 4344(1)$ Å^3, $Z = 4$, $R(|F|) = 0.057$ for 2329 data ($I/\sigma(I) \geq 3$), and 213 parameters; (**2**) monoclinic, *C*2/*c*, $a = 15.378(2)$ Å, $b = 14.172(2)$ Å, $c = 14.264(2)$ Å, $\beta = 99.10(1)°$, $V = 3069.5(7)$ Å^3, $Z = 4$, $R(|F|) = 0.075$ for 1147 data ($I/\sigma(I) \geq 3$), and 213 parameters; (**3**) monoclinic, *C*2/*c*, $a = 15.32(1)$ Å, $b = 14.19(1)$ Å, $c = 14.130(3)$ Å, $\beta = 99.41(3)°$, $V = 3031(3)$ Å^3, $Z = 4$, $R(|F|) = 0.085$ for 1133 data ($I/\sigma(I) \geq 3$) and 98 parameters. Complexes **2** and **3** are isotypes. In the three complexes, the centrosymmetric TETP macrocycle possesses a [3434] conformation; two propionate arms are extended, and the others are folded toward two protonated nitrogen atoms. The lanthanide coordination mode with the TETP ligand does not occur via the four nitrogen atom ring but only through carboxylic oxygen atoms belonging to four different ligands. Moreover, the four functionalized chains of the ligand are involved in the coordination polyhedron of the gadolinium and europium ions, but only extended propionate arms of TETP take part in the cerium ion coordination polyhedron, one of the oxygen atoms of asymmetric unit being bidentate between two metallic ions. In order to better understand the reactivity and the coordination scheme observed for these complexes, a theoretical study has been carried out using the molecular electrostatic potential as a tool to predict sites of the ligands where electrophilic attack should take place. The overall good agreement between calculated and observed structures permits us to explain the coordination scheme of this new class of complexes.

Introduction

The continued interest and research for new macrocyclic ligands stems mainly from their use as models for protein−metal binding sites in biological systems,[1] as selective complexants of metallic ions,[2−4] i.e. therapeutic reagents for the treatment of the metal toxicity,[5,6] radioactive waste water treatment,[7] functional groups for chelating ion-exchange materials,[8] and selective metal extractants in hydrometallurgy,[9] and to study host−guest interactions.[10] Tetraazamacrocycle ligands represent a class of macrocycles known for their ability to complex transition and non-transition metallic cations. The macrocyclic complexes of lanthanides are now currently used for other medical applications,[10] in radioimmunotherapy, in contrast-enhancing agents in magnetic resonance imaging (MRI), as NMR shift and relaxation reagents, and in many other novel clinical techniques.[10]

The main target in macrocyclic design is to synthesize macrocycles which are able to discriminate among the different metal cations. Many factors influence the selectivity of macrocycles toward the lanthanide cations and determine to some extent the structure of the formed complexes. In this study we focus on a particular class of macrocyclic ligand which has been used as complexants of lanthanide ions in aqueous solutions: namely, the *N*-tetrapropionate (acetate)-substituted tetraazamac-

* To whom correspondence should be addressed.
† Université Henri Poincaré.
‡ Université de Bourgogne.
§ Centre du Commissariat à l'Energie Atomique de Valduc, France.
⊗ Abstract published in *Advance ACS Abstracts,* July 15, 1997.

(1) (a) Kimura, E. *Pure Appl. Chem.* **1993**, *65*, 355. (b) *Environmental Inorganic Chemistry*; Martell, A. E., Irgolic, K. J., Eds.; VCH Publishers: Deerfield Beach, FL, 1985.
(2) Blain, S.; Appriou, P.; Chaumeil, H.; Handel, H. *Anal. Chim. Acta* **1990**, *232*, 331.
(3) Tsubuke, H.; Yoden, T.; Iwachido, T.; Zenki, M. *J. Chem. Soc., Chem. Commun.* **1991**, 1069.
(4) Handel, H. F.; Muller, R.; Guglielmetti, R. *Helv. Chim. Acta* **1983**, *66*, 514.
(5) Bullman, R. A. *Struct. Bonding* **1987**, *67*, 91.
(6) Bryce-Smith, D. *Chem. Soc. Rev.* **1986**, *15*, 93.
(7) Chollet, H. Utilisation de Macrocycles Tétraazotés pour la complexation des actinides en milieu aqueux. Validation pour le retraitement des effluents liquides aqueux. Ph.D. Thesis, Université de Bourgogne, 1994.
(8) Sahni, S. K.; Reedijk, J. *Coord. Chem. Rev.* **1984**, *1*, 59.
(9) Green, B. R.; Hancock, R. D. *J. S. Afr. Inst. Min. Metall.* **1982**, *82*, 303.
(10) Alexander, V. *Chem. Rev.* **1995**, *95*, 273. Lauffer, R. B. *Chem. Rev.* **1987**, *87*, 901. Tweedle, M. F. In *Lanthanides Probes in Life, Chemical and Earth Sciences*; Bunzli, J.-C. G., Chopin, G. R., Eds.; Elsevier: New York, 1989.

S0020-1669(96)00934-2 CCC: $14.00

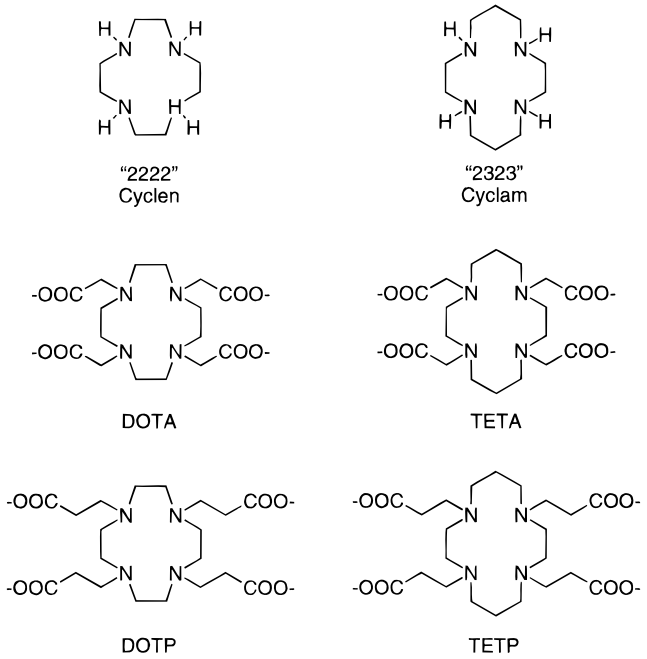

Figure 1. Formula schemes of free and N-substituted tetraazamacrocyclic ligands (DOTA, DOTP, TETA, TETP).

rocycles (Figure 1). It is well-known that the carboxyl groups appended to the macrocyclic ring can strongly enhance the stability of the complexes of these ligands. The DOTA ligand, for example, forms the most stable lanthanide complexes currently known, log $K(H_2O)$ being in the range 22.86−29.2.[11] This type of macrocycle with carboxyl N-substituent arms continues to be of interest to many chemists because they present a great selectivity toward metallic cations. However a detailed understanding of the mechanisms of the complexation reactions and also of the factors that determine the complex stability has not yet been achieved. The lanthanide *N*-tetrapropionate (acetate)-substituted tetraazamacrocycle complexes which are reported in this study present a diversity of structural geometries and coordinating schemes which we have attempted to rationalize and correlate to some physical parameters.

In an attempt to assess the significance of each of the parameters which might have induced the observed remarkable structural differences of the lanthanide−macrocyclic complexes, molecular mechanics and density functional theory calculations have been carried out in order to determine the molecular electrostatic potentials[12,13] of the macrocyclic ligands. This information complements the X-ray data. In the present study we classify three parameters which, in our opinion, strongly influence the coordination mode. These are the size of the macrocycle, the length of the appended arms, and the degree of protonation of the ligand.

Experimental Section

Reagents. Reagents grade $Ce(NO_3)_3{\cdot}6H_2O$, $Eu(NO_3)_3{\cdot}6H_2O$, and $Gd(NO_3)_3{\cdot}5H_2O$ (Janssen) were used as received without further purification to prepare the macrocyclic complexes.

Synthesis of H_4TETP (1,4,8,11-Tetrakis(2-carboxyethyl)-1,4,8,-11-tetraazacyclotetradecane). A solution of acrylic acid in pure ethanol (28.0 g; 0.39 mol) was added to a solution of cyclam (4 g; 0.02 mol) in the same solvent (150 mL). The solution was stirred at room temperature for 1 h, and the mixture was refluxed for 2 h. During heating a white solid is formed, and the reaction mixture was allowed to reflux for an additional 2 h. The solid was filtered off, washed several times with ethanol and ether, and dried under vacuum for 4 h at 1 mmHg/20 °C (yield: 80%). Colorless crystals have been prepared by slow evaporation at room temperature of a 0.04 M water solution of the corresponding compound.

^{1}H NMR (D_2O), δ (ppm): 1.9 (4H, q); 2.6 (8H, t); 2.8 (8H, t); 3.0 (8H, t); 3.1 (8H, s). ^{13}C NMR (D_2O), δ (ppm): 24.0; 33.2; 50.3; 51.0; 51.9; 180.1. Anal. Calcd for $C_{22}N_4O_8H_{40}{\cdot}CH_3CH_2OH$ (534.66): C, 53.9; H, 8.7; N, 10.5. Found: C, 53.0; H, 8.6; N, 10.6.

Synthesis of $[Ce(H_2TETP)](OH)(H_2O){\cdot}10H_2O$ (1). The synthesis of the Ce(III) TETP (1,4,8,11-tetrakis(2-carboxyethyl)-1,4,8,11-tetraazacyclotetradecane acid) complex has been carried out by reacting a 0.04 M water solution of H_4TETP with an equimolar water solution of cerium nitrate, $Ce(NO_3)_3{\cdot}6H_2O$ and heating at 80−90 °C until the solution was clear (about 5 min). The pH of the solution during the metalation reaction was monitored using a SCHOTT (CG 840 B) pH meter. The pH varied in the range 3.2 to 4.4 at the end of the reaction (about 5−6 h). Colorless crystals of $[(H_2TETP,Ce(III))^+,OH^-,H_2O{\cdot}10H_2O]$ were obtained by slow evaporation of the reaction mixture at room temperature.

Anal. Found for $CeC_{22}N_4O_{10}H_{41}{\cdot}10H_2O$: C, 28.0; H, 6.4; N, 6.9; Ce, 15.3. Calcd: C, 31.4; H, 7.3; N, 6.7; Ce, 16.6.

Synthesis of $[Gd(H_3TETP)](OH)_2(H_2O)_2{\cdot}3H_2O$ (2). The synthesis of the Gd(III) TETP (1,4,8,11-tetrakis(2-carboxyethyl)-1,4,8,11-tetraazacyclotetradecane acid) complex has been carried out by reacting a 0.04 M buffered solution (acetic acid/sodium acetate = 1/1) of H_4TETP with an equimolar solution of gadolinium nitrate, $Gd(NO_3)_3{\cdot}5H_2O$, prepared in the same buffered solution and heating at 80−90 °C until the solution was clear (about 5 min). The pH of the solution during the metalation reaction was monitored using a SCHOTT (CG 840 B) pH meter. The pH varied in a range from 3.5 to 3.8 at the end of the reaction (about 5−6 h) which indicates that the used buffer was not strong enough to stabilize the pH at the initial 4.75 value. Colorless crystals of $[(H_3TETP,Gd(III))^{2+},2OH^-,2H_2O{\cdot}3H_2O]$ were obtained by slow evaporation of the reaction mixture at room temperature.

Anal. Found for $GdC_{22}N_4O_{12}H_{45}{\cdot}3H_2O$: C, 33.9; H, 6.2; N, 8.9; Gd, 18.9. Calcd: C, 34.3; H, 6.6; N, 7.3; Gd, 20.4.

Synthesis of $[Eu(H_3TETP)](OH)_2(H_2O)_2{\cdot}3H_2O$ (3). The synthesis of the Eu(III) TETP (1,4,8,11-tetrakis(2-carboxyethyl)-1,4,8,11-tetraazacyclotetradecane acid) complex has been carried out by reacting a 0.04 M buffered solution (acetic acid/sodium acetate = 1/1) of H_4TETP with an equimolar solution of europium nitrate, $Eu(NO_3)_3{\cdot}6H_2O$, prepared in the same buffered solution and heating at 80−90 °C until the solution was clear (about 5 min). The pH of the solution during the metalation reaction was monitored using a SCHOTT (CG 840 B) pH meter. The pH varied in a range from 3.5 to 3.8. Colorless crystals of $[(H_3TETP,Eu(III))^{2+},2OH^-,2H_2O{\cdot}3H_2O]$ were obtained by slow evaporation of the reaction mixture at room temperature.

Anal. Found for $EuC_{22}N_4O_{12}H_{45}{\cdot}3H_2O$: C, 33.7; H, 6.1; N, 8.6; Eu, 17.2. Calcd: C, 34.6; H, 6.7; N, 7.3; Eu, 19.9.

X-ray crystallography. As crystals of complex **2** are very unstable when extracted from solution, it was necessary to mount the chosen crystal in a capillary with a drop of mother liquor. Crystals of **3** are also very unstable and were mounted with grease on a glass fiber and quickly cooled at 110 K under the nitrogen flow on an Enraf-Nonius low-temperature system. Crystals of **1** were more stable, and the X-ray data were collected at room temperature, without a capillary.

Quick data collections on a CAD4F diffractometer showed that all the complexes crystallized in the monoclinic system, space group *Cc* or *C*2/*c* (systematic absences: *hkl*, $h + k \neq 2n$; *h*0*l*, $l \neq 2n$). The unit cell parameters were obtained by least-squares fits to the observed setting angles of the Mo Kα_1 peaks of 25 reflections ($11° < 2\theta < 23°$ for **1**, $16° < 2\theta < 24°$ for **2**, and $11° < 2\theta < 22°$ for **3**). Crystal data and details of the data collections are reported in Table 1.

The DREAR programs[14] were used for the data reduction. After profile analysis, the data were corrected for Lorentz and polarization effects. No absorption correction was applied. Standard reflections,

(11) Izatt, R. M.; Pawlak, K.; Bradshaw, J. S.; Bruening, R. L. *Chem. Rev.* **1991**, *91*, 1721.
(12) *Chemical Applications of Atomic and Molecular Potentials*; Politzer, P., Truhlar, D. G., Eds.; Plenum Press: New York, 1981.
(13) Tomasi, J.; Bonaccorsi, R.; Cammi, R. In *Theoretical models of chemical bonding;* Maksic, Z., Ed.; Springer Verlag: New York, 1991; Vol. IV, p 229.
(14) Blessing, R. H. *Crystallogr. Rev.* **1987**, *1*, 3.

Table 1. Crystal Data and Data Collection Details for **1**−**3**

	1	**2**	**3**
molecular formula	$CeC_{22}N_4O_{20}H_{61}$	$GdC_{22}N_4O_{15}H_{51}$	$EuC_{22}N_4O_{15}H_{51}$
M_r	841.8	768.9	763.6
system	monoclinic	monoclinic	monoclinic
space group	*C*2/*c*	*C*2/*c*	*C*2/*c*
a (Å)	29.523(4)	15.378(2)	15.32(1)
b (Å)	17.492(3)	14.172(2)	14.19(1)
c (Å)	8.509(1)	14.264(2)	14.130(3)
β (deg)	98.72(1)	99.10(1)	99.41(3)
V (Å^3)	4344(1)	3069.5(7)	3031(3)
Z	4	4	4
F(000)	1756	1580	1576
D_x (g.cm^{-3})	1.29	1.66	1.67
ρ_{obsd}	not measd	not measd	not measd
μ (cm^{-1})	11.3	22.3	21.4
data collcn temp (°C)	20	20	−163(3)
graphite-monochromated radiation	Mo Kα (λ = 0.7107 Å)	Mo Kα (λ = 0.7107 Å)	Mo Kα (λ = 0.7107 Å)
cryst size (mm^3)	0.30 × 0.14 × 0.06	0.30 × 0.10 × 0.06	0.28 × 0.08 × 0.04
scan type	$\omega/2\theta$	$\omega/2\theta$	$\omega/2\theta$
scan speed (deg min^{-1})	1.3−5.5	0.6−2.1	0.5−2.7
scan width (deg)	0.8+0.35tanθ	0.8+0.35tanθ	0.9+0.35tanθ
$((\sin\theta)/\lambda)_{max}$ (Å^{-1})	0.60	0.70	0.60
hkl limit	$-34 \le h \le 34$, $-16 \le k \le 20$, $0 \le l \le 10$	$-21 \le h \le 21$, $0 \le k \le 16$, $0 \le l \le 20$	$-17 \le h \le 18$, $-16 \le k \le 16$, $0 \le l \le 16$
detector aperture ($V \times H$) (mm^2)	6 × 3	6 × 4	6 × 4
std reflcns	(3$\bar{1}$2), (2$\bar{4}$0), (312)	(353), ($\bar{3}$31), ($\bar{2}$04), ($\bar{4}$00)	($\bar{2}$04), ($\bar{2}$24), (042), ($\bar{3}3\bar{1}$)
no. of reflcns collcd	6529	4595	8792
no. of obsd reflcns ($I \le 3\sigma(I)$)	2329	1147	1133
no. of ls params	213	213	98
R; R_w; S[a]	5.7; 5.7; 1.46	7.5; 6.1; 2.41	8.5; 8.5; 2.18
w	$1.77/[\sigma^2(\lvert F\rvert) + 0.001\lvert F\rvert^2]$	$9.10/[\sigma^2(\lvert F\rvert) + 0.0002\lvert F\rvert^2]$	$3.95/[\sigma^2(\lvert F\rvert) + 0.001\lvert F\rvert^2]$
largest final shift (Δ/σ)	0.04	0.71 (U_{13}(W12))	0.27
largest e$^-$ density hole (e/A^3)	−1.09	−0.77	−1.45
largest e$^-$ density peak (e/A^3)	1.37 (x = 0.5; y = 0.3767; z = 0.75)	1.03 (x = 0.0; y = 0.2222; z = 0.25)	1.77 (x = 0.0223; y = 0.2825; z = 0.2947)

[a] $R = (\sum[K^{-1}|F_o(\vec{H})| - |F_c(\vec{H})|])/(\sum|F_o(\vec{H})|)$, $R_w = ((\sum w(\vec{H})[K^{-1}|F_o(\vec{H})| - |F_c(\vec{H})|]^2)/(\sum w(\vec{H})|F_o(\vec{H})|^2))^{1/2}$, and $S = ((\sum w(\vec{H})[K^{-1}|F_o(\vec{H})| - |F_c(\vec{H})|^2)/(u - up))^{1/2}$ with $w(H)) = k/(\sigma^2(F_o(H)))$ and $\sigma^2(F_o(\vec{H})) = \sigma^2_{count} + pF_o^2(H)$.

monitored every 2 h, showed a linear decay of about 4% and 5% for **1** and **2**, respectively. The standard reflections of **3** did not present a decay between the beginning and the end of the measurement, but their behavior as a function of time showed discontinuities due to reorientations of the specimen crystal during the data collection. For the three complexes these fluctuations were corrected. Of the 6529 reflections collected for **1**, 3818 were unique; 2137 were multiple measurements which on averaging gave an internal agreement $R_{int} = \sum(|F^2 - \langle F^2\rangle|/|F^2|) = 0.028$. For complex **2**, 4595 reflections were collected including 154 multiple measurements, giving rise to 4210 unique reflections (R_{int} = 1.5%). A total of 8792 reflections were collected for **3**, with 2627 multiple measurements ($R_{int}(F^2)$ = 7%, 2678 unique reflections). Only data with $I \ge 3\sigma(I)$ were used for the three structure determinations and least-squares refinements. These crystal structures were determined by Patterson function and difference Fourier maps.

The structure of complex **1** is centered, the macrocyclic ligand being on the [$^1/_4$, $^1/_4$, $^1/_2$] inversion center. Therefore, this complex has been refined in the *C*2/*c* space group. After location of all non-H atoms of the macrocycle, difference electron density maps revealed six residual peaks. These peaks which can be attributed to oxygen atoms of water molecules or hydroxylic ions (O5, W1, W2, W3, W4, W5) were taken into account in the refinement. One of these oxygen atoms (O5) is coordinated to the cerium ion at 2.498(8) Å. The two H atoms of W1 and W2 and one of the H atoms of W4 have been found from difference Fourier maps. Almost all hydrogen atoms of the macrocycle carbon atoms appeared in difference maps, the other ones being calculated according to standard conformation (d(C−H) = 1.08 Å).[15] No residual peak close to any carboxyl oxygen atom has been detected in the difference Fourier maps.

The structure of **2** clearly appeared to be centrosymmetric, with the TETP macrocycle located on the [$^1/_4$, $^3/_4$, $^1/_2$] inversion center. The molecular structure has been refined in the *C*2/*c* space group. Difference electron density maps showed, after location of all non-H atoms, four residual peaks, which were attributed to oxygen atoms of water molecules or hydroxylic ions (O5, W1, W2, W3) and were taken into account in the refinement. Two of these oxygen atoms (O5 and W1) are coordinated to the gadolinium ion. The W1 and W3 atoms, and one of the carboxyl oxygen atoms (O4), showed isotropic mean-square displacements unusually high compared to those of other atoms of the complex. Moreover, a difference Fourier map revealed a residual peak located at a short distance of each of the O4 and W1 oxygen atoms, in relation with atomic disorder. Therefore, the atomic positions of O4 and W1 are split (O41, O42 and W11, W12, respectively), with a multiplicity factor of 50%. Furthermore, the short distance between the W3 atom and its image by the 2-fold axis (2.11(5) Å) led us to attribute a multiplicity factor of 50% to W3. These results may contradict the *C*2/*c* space group hypothesis; then structure refinements were carried out in the *Cc* group, and this latter refinement did not bring any improvement. Therefore the *Cc* hypothesis was rejected. All methyl hydrogen positions were calculated according to standard conformation (d(C−H) = 1.08 Å).[15] Neither H atoms bound to carboxyl oxygen atoms nor those of water molecules were found in difference electron density maps.

Complex **3** is isotypal to **2**, and difference electron density map of **3** also revealed, after location of all non-H atoms, the same residual peaks found in **2** attributed to oxygen atoms of water solvate molecules or hydroxylic ions; the same atoms as before (O4, W1, W3) showed atomic position disorders.

SHELX76[16] and ORTEP[17] programs were used for structure refinements and drawings. Scattering factors were taken from refs 16 and

(15) Allen, F. *Acta Crystallogr.* **1986**, *B42*, 515.

(16) Sheldrick G. M. SHELX76, Program for Crystal Structure Determination, University of Göttingen, Germany, 1976.

(17) Johnson C. K. *ORTEP, Report ORNL-3794*, 2nd revision; Oak Ridge National Laboratory: Oak Ridge, TN, 1970.

Table 2. Positional and Equivalent Isotropic Thermal[a] Parameters and Their Estimated Standard Deviations for [Ce(H_2TETP)](OH)(H_2O)·10H_2O (**1**), [Gd(H_3TETP)](OH)$_2$(H_2O)$_2$·3H_2O (**2**), and [Eu(H_3TETP)](OH)$_2$(H_2O)$_2$·3H_2O (**3**)

atom	*x*	*y*	*z*	B_{eq} (Å^2)	atom	*x*	*y*	*z*	B_{eq} (Å^2)
				Compound **1**					
Ce	0.5	0.49093(4)	0.75	1.71(2)	C11	0.2017(3)	0.3747(6)	0.134(1)	3.6(3)
N1	0.3016(2)	0.3731(4)	0.4459(9)	2.5(2)	O1	0.4580(2)	0.4674(3)	0.4851(7)	2.7(1)
N2	0.2095(2)	0.3771(4)	0.5010(9)	2.7(2)	O2	0.4164(2)	0.4585(4)	0.2502(7)	2.7(1)
C1	0.2890(3)	0.4260(5)	0.572(1)	3.3(2)	O3	0.2441(2)	0.3839(4)	0.1701(8)	3.9(2)
C2	0.2448(3)	0.4013(5)	0.628(1)	3.1(2)	O4	0.1838(3)	0.3375(6)	0.014(1)	5.8(3)
C3	0.1710(3)	0.3404(5)	0.568(1)	3.4(2)	O5	0.4553(3)	0.3774(4)	0.8178(9)	4.2(2)
C4	0.1821(3)	0.2610(5)	0.630(1)	3.0(2)	W1	0.7007(3)	0.3183(5)	0.539(1)	5.2(2)
C5	0.1885(3)	0.2064(5)	0.496(1)	2.8(2)	W2	0.6235(3)	0.4004(5)	0.5525(9)	5.2(2)
C6	0.3393(3)	0.4072(5)	0.366(1)	2.6(2)	W3	0.5622(6)	0.7313(8)	0.667(3)	10.7(6)
C7	0.3844(3)	0.4110(5)	0.476(1)	2.9(2)	W4	0.4063(5)	0.831(1)	0.583(3)	11.4(6)
C8	0.4203(3)	0.4483(5)	0.3961(9)	2.3(2)	W5	0.528(1)	0.228(1)	0.592(5)	17(1)
C9	0.1922(3)	0.4404(5)	0.395(1)	3.2(2)	HN1[b]	0.2730	0.3765	0.3697	3.5
C10	0.1695(3)	0.4121(6)	0.232(1)	3.7(3)					
				Compound **2**					
Gd	0.5	0.7388(1)	0.25	5.59(4)	C11	0.4526(9)	0.631(1)	0.447(1)	5.0(2)
N1	0.2258(7)	0.5528(8)	0.4728(6)	3.3(2)	O1	0.2489(7)	0.2281(8)	0.3636(7)	5.7(2)
N2	0.3465(8)	0.6507(8)	0.6106(7)	3.1(2)	O2	0.1282(7)	0.3150(8)	0.3215(8)	5.9(2)
C1	0.231(1)	0.528(1)	0.5742(9)	4.6(2)	O3	0.3867(6)	0.5850(7)	0.4129(6)	4.3(2)
C2	0.270(1)	0.606(1)	0.6428(9)	4.1(2)	O41	0.510(1)	0.648(2)	0.400(1)	5.4(3)
C3	0.3734(9)	0.733(1)	0.6711(8)	4.0(2)	O42	0.482(1)	0.706(2)	0.406(2)	7.7(3)
C4	0.317(1)	0.819(1)	0.6478(9)	4.2(2)	O5	0.1151(8)	0.1204(7)	0.2697(8)	5.8(2)
C5	0.3286(9)	0.8607(9)	0.554(1)	3.0(2)	W11	0.453(1)	0.835(1)	0.368(1)	3.6(3)
C6	0.189(1)	0.469(1)	0.4119(9)	3.8(2)	W12	0.477(2)	0.931(2)	0.307(2)	10.4(3)
C7	0.250(1)	0.386(1)	0.421(1)	4.3(2)	W2	0.073(1)	0.659(1)	0.063(1)	11.2(3)
C8	0.204(1)	0.304(1)	0.365(1)	3.7(2)	W3	0.460(2)	1.030(2)	0.304(2)	9.4(3)
C9	0.4214(9)	0.584(1)	0.6134(9)	3.4(2)	HN1[b]	0.2709	0.5611	0.4596	4.4
C10	0.4860(9)	0.623(1)	0.554(1)	4.8(2)					
				Compound **3**					
Eu	0.5	0.7337(2)	0.25	4.03(6)	C11	0.455(1)	0.626(2)	0.450(1)	3.1(4)
N1	0.2243(9)	0.552(1)	0.474(1)	1.3(3)	O1	0.2508(9)	0.227(1)	0.364(1)	3.2(3)
N2	0.344(1)	0.652(1)	0.613(1)	1.6(3)	O2	0.129(1)	0.313(1)	0.323(1)	3.4(3)
C1	0.228(1)	0.529(2)	0.576(1)	2.5(4)	O3	0.3839(9)	0.582(1)	0.4136(9)	2.5(3)
C2	0.269(1)	0.608(1)	0.645(1)	1.8(3)	O41	0.508(1)	0.646(2)	0.402(2)	1.0(4)
C3	0.371(1)	0.733(2)	0.674(1)	2.4(3)	O42	0.481(3)	0.705(3)	0.408(3)	7.0(7)
C4	0.316(1)	0.821(1)	0.649(1)	1.7(3)	O5	0.120(1)	0.118(1)	0.268(1)	3.7(3)
C5	0.330(1)	0.859(1)	0.555(1)	2.1(4)	W11	0.454(1)	0.834(2)	0.371(1)	1.1(4)
C6	0.190(1)	0.470(1)	0.411(1)	2.0(3)	W12	0.478(3)	0.935(4)	0.309(3)	9.9(7)
C7	0.252(1)	0.385(2)	0.421(1)	2.8(4)	W2	0.075(1)	0.660(1)	0.062(1)	6.9(4)
C8	0.207(1)	0.302(1)	0.365(1)	2.3(4)	W3	0.452(2)	1.022(2)	0.311(2)	3.1(5)
C9	0.419(1)	0.583(1)	0.619(1)	2.2(4)	HN1[b]	0.2703	0.5532	0.4695	1.6
C10	0.485(1)	0.620(2)	0.558(1)	2.8(4)					

[a] $B_{eq} = (4/3)[a^{*2}B(1,1) + b^{*2}B(2,2) + c^{*2}B(3,3) + a^*b^*(\cos\gamma^*)B(1,2) + a^*c^*(\cos\beta^*)B(1,3) + b^*c^*(\cos\alpha^*)B(2,3)]$. [b] Hydrogen atom involved in the intramolecular hydrogen bond.

18. In refinements of **1** and **2**, the parameters included anisotropic mean-square displacements for the non-H atoms, whereas, for complex **3**, these displacement parameters have been refined using the isotropic model, due to the poor data quality. All hydrogen atoms were included as a fixed contribution to the refinement process, H isotropic mean-square displacements being $B(H) = 1.3B(X)$, where $B(X)$ is the equivalent isotropic mean-square displacement for atom X to which the H atom is covalently bound.

Positional and equivalent isotropic thermal parameters for **1**−**3** are reported in Table 2. Macrocycle bond distances and valence angles are listed in Table 3, and torsional angles, in Table 4. Distances and angles of lanthanide ion coordination polyhedrons are given in Table 5, and the geometric data for the intramolecular hydrogen bonds in the TETP ligand, in Table 6.

Molecular Modeling: Molecular Electrostatic Potentials. During the last 50 years a dominant theme of theoretical chemistry has been the search for methods able to predict the chemical behavior of chemical entities. Many indices of reactivity like atomic charges, bond orders, free valences, frontier electron densities, Fukui functions, and the molecular electrostatic potentials (MEP) have been introduced. The shape of MEP is considered now as a standard tool in quantum chemistry for the analysis of the reactivity of molecules.[12,13,19−22] Unlike many of the other quantities used as reactivity indices, the MEP is a real physical property which can be either determined experimentally by X-ray and electron diffraction methods[23−25] or calculated from the wave function. Its interpretation is simple in terms of classical electrostatics: The molecule provides a potential around itself which is felt by another approaching chemical species.

Any charge distribution creates a potential $V(\mathbf{r})$ in the space as defined by

$$V(\mathbf{r}) = \sum_i Z_i/|\mathbf{R}_i - \mathbf{r}| - \int \rho(\mathbf{r}')\, d\mathbf{r}'/|\mathbf{r}' - \mathbf{r}|$$

where Z_i is the charge on nucleus i located at $\mathbf{R}_i$ and $\rho(\mathbf{r})$ is the electron

(18) *International Tables for X-ray Crystallography*; Kluwer: Boston, MA, Vol. IV.

(19) Korchowiec, J.; Gerwens. H.; Jug, K. *Chem. Phys. Lett.* **1994**, *222*, 58.
(20) Mishra, P. C.; Kumar, A. *Top. Curr. Chem.* **1995**, *174*, 27.
(21) Naray-Szabo, G.; Ferenczy, G. G. *Chem. Rev.* **1995**, *95*, 829.
(22) Murray, J. S.; Brinck, T.; Grice, M. E.; Politzer, P. *J. Mol. Struct.* **1992**, *256*, 29.
(23) Lecomte, C. *Adv. Mol. Struct. Res.* **1995**, *1*, 261.
(24) Ghermani, N. E.; Lecomte, C.; Bouhmaida, N. *Z. Naturforsch.* **1993**, *48a*, 91.
(25) Ghermani, N. E.; Bouhmaida, N.; Lecomte, C.; Papet, A.-L.; Marsura, A. *J. Phys. Chem.* **1994**, *98*, 6287.

Table 3. Bond Distances (Å) and Angles (deg) in the TETP Macrocycle of **1**−**3** with Esd's in Parentheses

	1	**2**	**3**
N1−C1	1.50(1)	1.48(2)	1.47(2)
N1−C5′	1.49(1)	1.50(2)	1.53(2)
N1−C6	1.51(1)	1.52(2)	1.50(2)
N2−C2	1.44(1)	1.47(2)	1.44(3)
N2−C3	1.49(1)	1.47(2)	1.46(3)
N2−C9	1.47(1)	1.49(2)	1.51(3)
C1−C2	1.52(1)	1.53(2)	1.55(3)
C3−C4	1.50(1)	1.50(2)	1.52(3)
C4−C5	1.52(1)	1.50(2)	1.48(3)
C6−C7	1.51(1)	1.51(2)	1.53(3)
C7−C8	1.49(1)	1.51(2)	1.52(3)
C9−C10	1.53(1)	1.51(2)	1.51(3)
C10−C11	1.50(2)	1.53(2)	1.52(3)
C8−O1	1.291(8)	1.28(2)	1.26(3)
C8−O2	1.24(1)	1.24(2)	1.24(2)
C11−O3	1.26(1)	1.24(2)	1.28(3)
C11−O41	1.26(1)	1.22(3)	1.18(3)
C11−O42		1.33(3)	1.36(5)
C1−N1−C5′	113.2(7)	112(1)	112(1)
C1−N1−C6	110.8(6)	110(1)	111(1)
C5′−N1−C6	113.3(6)	110.6(9)	111(1)
C2−N2−C3	110.2(8)	109(1)	109(2)
C2−N2−C9	112.4(7)	112(1)	110(2)
C3−N2−C9	110.2(7)	110(1)	110(1)
N1−C1−C2	111.3(7)	114(1)	114(2)
N2−C2−C1	114.1(8)	111(1)	113(2)
N2−C3−C4	113.2(7)	115(1)	114(1)
C3−C4−C5	111.2(8)	112(1)	111(2)
N1′−C5−C4	112.0(7)	114(1)	113(2)
N1−C6−C7	112.5(7)	113(1)	114(1)
C6−C7−C8	111.1(7)	109(1)	110(2)
O1−C8−O2	119.5(7)	124(1)	124(2)
O1−C8−C7	117.0(7)	116(1)	118(2)
O2−C8−C7	123.4(7)	120(1)	117(2)
N2−C9−C10	112.2(7)	109(1)	109(2)
C9−C10−C11	114.6(8)	116(1)	117(2)
O3−C11−O41	123(1)	120(2)	120(2)
O3−C11−O42		124(2)	121(2)
O3−C11−C10	120.1(9)	119(1)	119(2)
O41−C11−C10	116.9(9)	114(1)	118(2)
O42−C11−C10		115(1)	115(2)

density function of the given molecule. This equation contains a summation over the point charge of the nuclei and an integration over the "continuous" negative electron distribution. The sign of $V(\mathbf{r})$ at any point out of the molecular region reflects which of the nucleus (+) or the electron density (−) has a major effect.

One of the first applications of the MEP was to determine a reactivity map to explain and predict the sites of the electrophilic attack on a molecule. An approaching electrophile would be attracted to the negative $V(\mathbf{r})$ regions, particularly where $V(\mathbf{r})$ has local minima.[25] In the present study we have plotted the MEP to localize the more electronegative sites on some *N*-tetrapropionate(acetate)-substituted tetraazamacrocyclic ligands susceptible to attract the metallic cation.

The calculation of the MEP of a molecule is straightforward if its wave function or $\rho(\mathbf{r})$ is known. Most ab initio calculations of $V(\mathbf{r})$ have been based on the self-consistent-field (SCF) or near-Hartree−Fock wave functions and therefore do not consider the electron correlation. Efforts have been made to understand the effect of the electron correlation on the MEP, and contradictory conclusions have been reported[26−28] relative to its importance in deriving the electrostatic potentials. However, the overall pattern of the MEP for a given molecule is not greatly modified by the level of correlation used in the calculations. In addition to conventional ab initio and semiempirical methods for computing molecular properties, there is an increasing use

Table 4. Torsion Angles and Estimated Standard Deviations (deg) in the TETP Macrocycle of **1**−**3**[a]

	1	**2**	**3**
N1−C1−C2−N2	−42(1)	−42(2)	−40(2)
C1−C2−N2−C3	169.4(7)	172(1)	173(1)
C2−N2−C3−C4	−75(1)	−78(1)	−80(2)
N2−C3−C4−C5	−66(1)	−69(2)	−68(2)
C3−C4−C5−N1′	−178.7(7)	−180(1)	−180(1)
C4−C5−N1′−C1′	−172.4(7)	−165(1)	−165(2)
C5−N1′−C1′−C2′	63.8(9)	58(2)	59(2)
C2−C1−N1−C6	167.6(7)	178(1)	176(2)
C1−N1−C6−C7	68.7(9)	−67(1)	−67(2)
C4′−C5′−N1−C6	−60.4(9)	−72(1)	−70(2)
C5′−N1−C6−C7	−59.8(9)	168(1)	167(2)
N1−C6−C7−C8	−177.3(7)	174(1)	173(2)
C6−C7−C8−O1	−15(1)	178(1)	178(2)
C6−C7−C8−O2	167.9(7)	1(2)	−2(3)
C1−C2−N2−C9	−67(1)	−66(1)	−67(2)
C2−N2−C9−C10	158.3(8)	163(1)	163(2)
C4−C3−N2−C9	160.1(8)	159(1)	159(2)
C3−N2−C9−C10	−78(1)	−75(1)	−77(2)
N2−C9−C10−C11	−67(1)	−65(2)	−66(2)
C9−C10−C11−O3	−16(1)	−18(2)	−15(3)
C9−C10−C11−O41	166.6(9)	−169(2)	−173(2)
C9−C10−C11−O42		144(2)	139(3)

[a] The sign is positive if when looking from atom 2 to 3 a clockwise motion of atom 1 would superimpose it on atom 4.

of density functional theory.[29−34] This approach is based on the Hohenberg−Kohn theorem,[35] stating that all the electronic properties of a chemical system in its ground state, including energy, are determined by the electron density. An important feature of the DFT approach is that it takes into account the electron correlation, while requiring much less computer time and space than ab initio methods.

Despite the increasing power of the computers and the recent developments of highly effective algorithms, the complete optimization of the molecular structure of macrocyclic compounds studied in the present work remains a difficult task within a reasonable time, even if the DFT method is used for the calculation. The MEP strongly depends upon the conformation and configuration of the molecule. Indeed, each three-dimensional arrangement of atoms in a molecule corresponds to a different electronic distribution and hence a different MEP. Thus, it is fundamental to define the molecular geometry before calculating its electronic properties.

While relatively rigid compounds can exist only in a small number of conformations, flexible compounds such as tetraazamacrocycles can adopt a large variety of dynamically interconverting geometries. Therefore, it was necessary to explore the conformational energy hypersurface to locate the local minima and the global minimum. In the present study molecular mechanics and molecular dynamics (DISCOVER module of the BIOSYM Molecular Modeling Package on a Silicon Graphics Indigo2 workstation)[36] have been used to perform an exhaustive search to identify the low-energy conformers of the DOTA, DOTP, TETA, H_2TETP, and H_4TETP macrocyclic ligands. Our crystallographic data[37,38] have been used as benchmarks: The conformers determined by X-ray diffraction studies should be among the low-

(26) Price, S. L.; Andrews, J. S.; Murray, C. W.; Amos, R. D. *J. Am. Chem. Soc*. **1992**, *114*, 8268.
(27) Les, A.; Adamowicz, L. *Chem. Phys*. **1991**, *153*, 409.
(28) Wang, L. C.; Boyd, R. *J. Chem. Phys*. **1989**, *90*, 1083.
(29) Parr, R. G.; Yang, W. *Density Functional Theory of atoms and Molecules*; Oxford University Press: New York, Claredon, Oxford, 1989.
(30) Labanowski, J. K.; Andzelm W. *Density Functional Methods in Chemistry;* Springer-Verlag: New York, 1991.
(31) Salahub, D. R.; Castro, M.; Proynov, E. I. In *Relativistic and Electron Correlation Effects in molecules and solids*; Malli, G. L., Ed.; Plenum Press: New York and London, 1994.
(32) March, N. H. *Electron Density Theory of Atoms and Molecules;* Academic Press Inc.: San Diego, CA, 1992.
(33) Ziegler, T. *Chem. Rev*. **1991**, *91*, 651.
(34) *Modern Density Functional Theory. A Tool for Chemistry;* Seminario, J. M., Politzer, P., Eds.; Elsevier: Amsterdam, 1995.
(35) Hohenberg, P.; Kohn W. *Phys. Rev*. **1964**, *136*, B864.
(36) BIOSYM Technologies Inc., San Diego, CA, 1994 (Release 237).
(37) Dahaoui-Gindrey, V.; Lecomte, C.; Gros, C.; Mishra, A. K.; Guilard, R. *New J. Chem*. **1995**, *19*, 831.

Table 5. Distances and Angles of Lanthanide Ion Coordination Polyhedrons

Ce/TETP[a]			
Ce−O1(**1**)(**1′**)	2.437(5)	Ce−O2(**2**)(**2′**)	2.624(6)
Ce−O1(**2**)(**2′**)	2.613(6)	Ce−O5(**1**)(**1′**)	2.498(8)
O1(**1**)−Ce−O1(**1′**)	160.5(3)	O1(**2**)−Ce−O2(**2**)	49.4(2)
O1(**1**)−Ce−O1(**2**)	64.8(2)	O1(**2**)−Ce−O2(**2′**)	117.5(2)
O1(**1**)−Ce−O1(**2′**)	121.4(2)	O2(**2**)−Ce−O2(**2′**)	140.6(3)
O1(**1**)−Ce−O5(**1**)	82.3(2)	O5(**1**)−Ce−O5(**1′**)	74.7(3)
O1(**1**)−Ce−O5(**1′**)	82.2(2)	O5(**1**)−Ce−O1(**2**)	136.6(2)
O1(**1**)−Ce−O2(**2**)	113.8(2)	O5(**1**)−Ce−O1(**2′**)	73.6(2)
O1(**1**)−Ce−O2(**2′**)	73.2(2)	O5(**1**)−Ce−O2(**2**)	142.9(2)
O1(**2**)−Ce−O1(**2′**)	147.6(3)	O5(**1**)−Ce−O2(**2′**)	74.9(2)

	Gd/TETP	Eu/TETP
Gd(Eu)−O2(**1**)(**1′**)	2.34(1)	2.36(1)
Gd(Eu)−O41(**2**)	2.48(2)	2.47(2)
Gd(Eu)−O42(**3**)	2.33(2)	2.34(4)
Gd(Eu)−O5(**1**)(**1′**)	2.42(1)	2.44(2)
Gd(Eu)−W11(**2**)	2.36(2)	2.41(2)
Gd(Eu)−W12(**3**)	2.88(3)	3.01(5)

Gd/TETP[b]		Eu/TETP[b]	
O2(**1**)−Gd−O2(**1′**)	124.9(6)	O2(**1**)−Eu−O2(**1′**)	123.4(7)
O2(**1**)−Gd−O41(**2**)	86.0(5)	O2(**1**)−Eu−O41(**2**)	86.6(6)
O2(**1′**)−Gd−O41(**2**)	123.3(5)	O2(**1′**)−Eu−O41(**2**)	122.4(7)
O2(**1**)−Gd−O42(**3**)	106.7(6)	O2(**1**)−Eu−O42(**3**)	106(1)
O2(**1′**)−Gd−O42(**3**)	84.1(6)	O2(**1′**)−Eu−O42(**3**)	84(1)
O2(**1**)−Gd−O5(**1**)	73.7(4)	O2(**1**)−Eu−O5(**1**)	72.9(5)
O2(**1**)−Gd−O5(**1′**)	157.1(4)	O2(**1**)−Eu−O5(**1′**)	158.1(5)
O2(**1**)−Gd−W11(**2**)	75.7(5)	O2(**1**)−Eu−W11(**2**)	74.6(6)
O2(**1′**)−Gd−W11(**2**)	73.3(5)	O2(**1′**)−Eu−W11(**2**)	73.0(6)
O2(**1**)−Gd−W12(**2**)	63.4(5)	O2(**1**)−Eu−W12(**2**)	63(1)
O2(**1′**)−Gd−W12(**2**)	64.7(5)	O2(**1′**)−Eu−W12(**2**)	63(1)
O41(**2**)−Gd−O42(**3**)	136.0(8)	O41(**2**)−Eu−O42(**3**)	138(1)
O41(**2**)−Gd−O5(**1**)	66.2(6)	O41(**2**)−Eu−O5(**1**)	69.0(7)
O41(**2**)−Gd−O5(**1′**)	71.7(5)	O41(**2**)−Eu−O5(**1′**)	71.6(6)
O41(**2**)−Gd−W11(**2**)	70.8(7)	O41(**2**)−Eu−W11(**2**)	70.0(8)
O41(**2**)−Gd−W12(**3**)	137.7(8)	O41(**2**)−Eu−W12(**3**)	137(1)
O42(**3**)−Gd−O5(**1**)	77.1(6)	O42(**3**)−Eu−O5(**1**)	77(1)
O42(**3**)−Gd−O5(**1′**)	87.0(6)	O42(**3**)−Eu−O5(**1′**)	89(1)
O42(**3**)−Gd−W11(**2**)	152.7(7)	O42(**3**)−Eu−W11(**2**)	151(1)
O42(**3**)−Gd−W12(**3**)	83.1(8)	O42(**3**)−Eu−W12(**3**)	82(1)
O5(**1**)−Gd−O5(**1′**)	92.3(5)	O5(**1**)−Eu−O5(**1′**)	96.0(7)
O5(**1**)−Gd−W11(**2**)	128.1(5)	O5(**1**)−Eu−W11(**2**)	128.3(6)
O5(**1**)−Gd−W12(**3**)	124.5(5)	O5(**1**)−Eu−W12(**3**)	123(1)
O5(**1′**)−Gd−W11(**2**)	100.6(5)	O5(**1′**)−Eu−W11(**2**)	99.6(7)
O5(**1′**)−Gd−W12(**3**)	138.0(5)	O5(**1′**)−Eu−W12(**3**)	136(1)
W11(**2**)−Gd−W12(**3**)	73.7(7)	W11(**2**)−Eu−W12(**3**)	72(1)

[a] Symmetry codes: (**1**) *x*, *y*, *z*, (**1′**) 1 − *x*, *y*, $^3/_2$ − *z*; (**2**) 1 − *x*, 1 − *y*, 1 − *z*, (**2′**) *x*, 1 − *y*, $^1/_2$ + *z*. [b] Symmetry codes: (**1**) $^1/_2$ + *x*, $^1/_2$ + *y*, *z*, (**1′**) $^1/_2$ − *x*, $^1/_2$ + *y*, $^1/_2$ − *z*; (**2**) *x*, *y*, *z*; (**3**) 1 − *x*, *y*, $^1/_2$ − *z*.

Table 6. Geometry of the Intramolecular Three-Center Hydrogen Bond in the TETP Ligand for **1**−**3**

	1	**2**	**3**
N1···O3 (Å)	2.686(9)	2.78(1)	2.75(2)
N1···N2 (Å)	2.83(1)	2.84(1)	2.85(2)
N1−HN1···O3 (deg)	150.3(5)	175.2(7)	159(1)
N1−HN1···N2 (deg)	110.8(5)	100.2(8)	105(1)

energy conformers obtained from the calculations, and experimental structural features such as bond lengths and bond and torsion angles should be reproduced by the calculation. It is well-known that 12-membered ring cycles have a preferably [3333] quadrangular conformation, and 14-membered ring cycles prefer [3434] according to the Dale's nomenclature.[39] So we focused our attention on reproducing these features for all the calculated macrocycles.

We used the following strategy for the search of the conformational space in the vicinity of the low-energy conformers of the macrocyclic ligands: After building up the ligand, full matrix optimization was employed to obtain the starting conformer, which was used to initialize a molecular dynamics simulation at a relatively high temperature (600 K). A second set of optimization was started from the 5 lowest energy conformers found from the first search. This iterative procedure was repeated in successive runs until the lowest 5 conformers were found at least twice and until the features of the known crystal structures were reproduced by at least one conformer (torsion angles, intramolecular hydrogen bonds). Then these latter results were used as a starting point for the search of the low-lying minima for DOTA, H_2TETP, H_4TETP, TETA, and DOTP.

When the molecular structure of the ligand is determined by the molecular mechanics (dynamics) procedure, its MEP can be obtained from a single point DFT (Dmol)[36] calculation. All the calculations have been performed according to the experimental conditions and, particularly, the pH conditions which define the degree of protonation of the macrocyclic ligand. The results of these calculations are shown in Figures 3−5, 7, and 8. It should be noted that in our approach the MEP does not typically take into account changes such as polarization or geometry distortion occurring when the metal begins to interact with the ligand. Moreover, the MEP does not reflect the nature of the approaching species. Because of these inherent limitations, the MEP is most useful as a guide to study the early stages of a reaction where these effects are relatively minor.

Results and Discussion

X-ray Crystallography. ORTEP[17] views of the crystal structures and coordination polyhedrons of **1**−**3** are given in Figure 2 with the numbering scheme used. Since the three structures are centrosymmetric, only half of the atoms of the chemical formulas are unique.

Chemical Formula of 1. The N1−C bond distances are on average slightly longer than those of the N2 atom (1.50(1) and 1.47(2) Å, respectively). This is in agreement with a protonated N1 atom as already observed in our previous studies of the tetraprotonated, pentaprotonated, and octaprotonated TETP free ligand.[38] Furthermore, this assumption is confirmed by the presence of a residual peak of 0.5 e Å^{-3} at 0.98 Å from N1 on the difference Fourier map (average C−N−peak angle = 106°). This hydrogen is involved in a three-center hydrogen bond (see below). This peak which corresponds to the HN1 hydrogen atom was taken into account in the refinement. No residual peak appeared close to N2. The C−O bond lengths, statistically equal to 1.26(2) Å, are in favor of deprotonated carboxyl groups. Consequently, the deprotonation of the four carboxyl groups and the protonation of the two N1 nitrogen atoms demonstrate that TETP is diprotonated bearing two negative charges. Therefore, this ligand was named H_2TETP^{2-}. The cerium bearing a +3 charge indicates that one of the two related O5 atoms is a water molecule and the other a hydroxyl ion OH^-. Further assignments are limited by location of hydrogen atoms, which was not possible in this case. The proposed chemical formula for **1** is: $[Ce(III),H_2TETP]^+,OH^-,H_2O{\cdot}10H_2O$.

Chemical Formulas of 2 and 3. In **2** and **3**, the N1 nitrogen atom is protonated with N−C bond distance averages equal to 1.50(2) and to 1.48(2) Å in complex **2** and to 1.50(3) and 1.47(3) Å in complex **3**, for N1 and N2, respectively. Furthermore, the difference Fourier map shows a HN1 residual peak of 0.80 e Å^{-3} at 0.76 Å from N1 (average C−N1−HN1 angle = 108(3)°) in **2** and a HN1 residual peak of 0.93 e Å^{-3} at 0.72 Å from N1 (average C−N1−HN1 angle = 107(7)°) in **3**, which were taken into account in the refinements. No residual peak appeared close to N2. Examination of the C−O bond lengths

(38) Dahaoui-Gindrey, V.; Lecomte, C.; Chollet, H.; Mishra, A. K.; Mehadji, C.; Guilard, R. *New J. Chem.* **1995**, *19*, 839.

(39) Dale, J. *Isr. J. Chem.* **1980**, *20*, 3. The digits in the [3434] term designate the number of bonds between bends of the macrocycle which are genuine corners, two *gauche* bonds of the same sign located between two *anti* bonds defining the geometry of the corner.

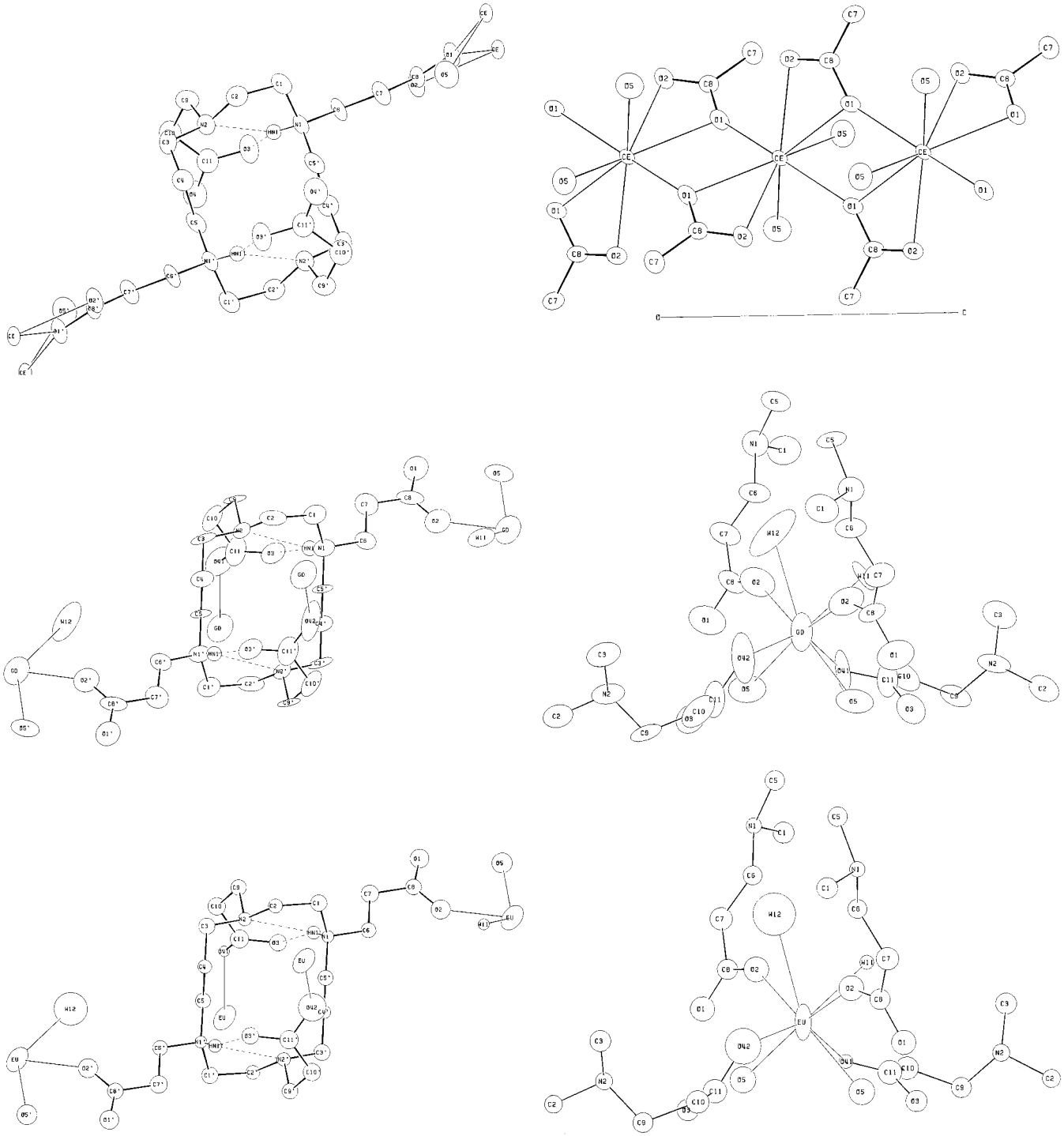

Figure 2. ORTEP[17] views of the crystal structures and coordination polyhedrons of (top to bottom) the Ce/TETP (**1**), Gd/TETP (**2**), and Eu/TETP (**3**) complexes with 50% probability thermal ellipsoids for non-H atoms. Atoms obtained by an inversion center have primed labels.

clearly shows that the extended (O1, C8, O2) carboxyl group is deprotonated with statistically equal C−O bond distances. As shown in the Experimental Section, the O4 atoms of the folded propionate arms are disordered (O41, O42). The corresponding C11−O4 distances agree either with a single bond (1.33(3) and 1.36(5) Å, for **2** and **3**, respectively, O4 ≡ O42) or with a double bond (1.22(3) and 1.18(3) Å, for **2** and **3**, respectively, O4 ≡ O41). Thus, this could lead to statistical equipartition of both COOH and COO^- groups. Protonation of the two N1 nitrogen atoms and deprotonation of three carboxyl groups show that the TETP macrocyclic ligand is triprotonated and bears one negative charge. So, this ligand is named H_3TETP^-. In view of the synthesis mode of both complexes **2** and **3**, the expected metallic ion oxidation state is III. As discussed above for **1**, one oxygen atom of the asymmetric unit must therefore be an OH^- ion. The most probable hypothesis would be that the coordinated O5 oxygen atom, which does not present any positional disorder, is the OH^- ion. In conclusion, the chemical formulas we may suggest are $[Gd(III),H_3TETP]^{2+},2OH^-,2H_2O{\cdot}3H_2O$ for **2**, and $[Eu(III), H_3TETP]^{2+},2OH^-,2H_2O{\cdot}3H_2O$ for **3**. However, these formulas are based on an interpretation of a disordered COO (COOH) group, and therefore, we cannot exclude the $[Gd(Eu),H_2TETP]^+,OH^-,3H_2O{\cdot}3H_2O$ hypothesis.

Coordination Mode of the Lanthanide Ions in the Three Complexes. Contrary to what was expected by comparison to

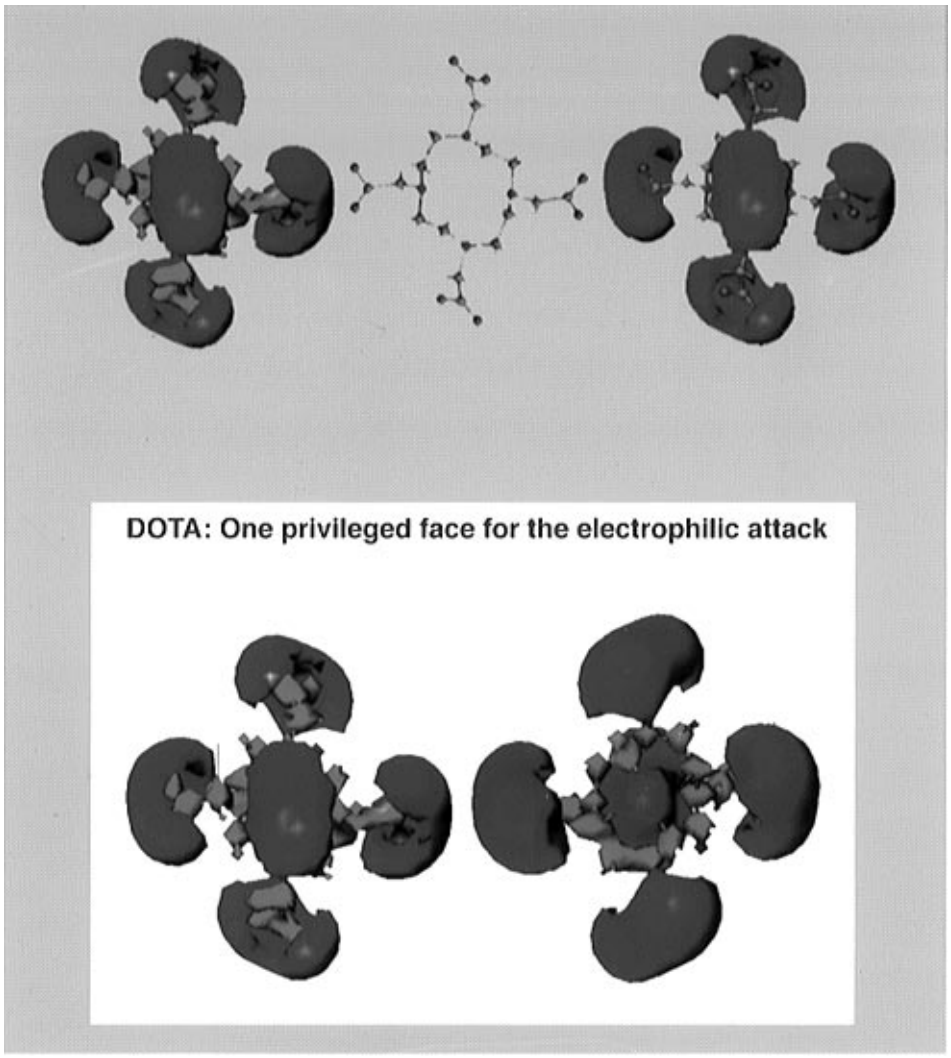

Figure 3. MEP and molecular structure of the DOTA ligand. The blue (red) surfaces correspond to the negative (positive) potential regions. The contour level used to plot the MEP surfaces has been chosen at 0.3 au.

the TETA/Tb,[40] DOTA/Gd,[41] and DOTA/Eu[42] complexes, the lanthanide ions are not coordinated to the TETP macrocyclic ligand via its four nitrogen atoms and its four carboxyl groups. In the TETP complexes, the metallic ions are coordinated to the ligand only via oxygen atoms belonging to four different macrocyclic ligands.

In **1,** the four H_2TETP molecules are linked to the cerium ion via their extended propionate groups only: As shown in Figure 2, two of the TETP ligands participate in the coordination polyhedron by the two oxygen atoms of their carboxyl group (Ce−O1 = 2.613(6) Å; Ce−O2 = 2.624(6) Å), whereas the two others are coordinated to the metallic ion by only one oxygen (Ce−O1 = 2.437(5) Å); the O1 oxygen atom acts as a bidentate ligand coordinate, binding two cerium ions related by an inversion center. As discussed above, the coordination polyhedron is completed by one hydroxyl ion and one water molecule. Therefore, the cerium ion is eight-coordinated. The four oxygen atoms [O1(**2**: $1-x, 1-y, 1-z$), O1(**2′**: $x, 1-y, {}^1/_2+z$), O2(**2**), O2(**2′**)] are coplanar and the cerium ion lies 0.8 Å above the plane. The four other oxygen atoms are located at 1.2 Å (O1(**1**: x, y, z), and O1(**1′**: $1-x, y, {}^3/_2-z$)) and 2.8 Å (O5(**1**) and O5(**1′**)) above this plane, the [Ce,O5(**1**),O5(**1′**)] plane being perpendicular to the [Ce,O1(**1**),O1(**1′**)] plane. The structure of this complex, where the metallic ion is only coordinated via carboxylic oxygen atoms of only two of the four functionalized chains, is similar to that of the recently reported[43] $[Mg(H_2TETA)(H_2O)_4]\cdot 4H_2O$ complex.

As seen in Figure 2, the four functionalized chains of the ligand in **2** and **3** are involved in the coordination polyhedron of the gadolinium and europium ions, by only one of the two oxygen atoms of the carboxyl groups. As discussed above, the lanthanide coordination polyhedron is completed by two hydroxyl groups and by two water molecules.

Conformational Similarities of the TETP Ligand in the Three Complexes. Since the TETP macrocycle cavity does not coordinate the lanthanide ions, the cyclam skeleton has, as expected, the stable conformation of the free ligand, that is the quadrangular [3434] conformation. The torsion angle values, given in Table 4, are close to those found in the free TETP[38] ligand, in TETPA (1,4,8,11-tetrakis(2-carbamoylethyl)-1,4,8,-11-tetraazacyclotetradecane),[37] and in *N*-tetrapropionic methyl ester.[44] Moreover, both propionate arms linked to the protonated

(40) Spirlet, M.-R.; Rebizant, J.; Loncin, M.-F.; Desreux, J. F. *Inorg. Chem.* **1984**, *23*, 4278.
(41) Dubost, J.-P.; Leger, J.-M.; Langlois, M.-H.; Meyer, D.; Schaefer, M. *C. R. Acad. Sci. Paris* **1991**, *312* (II), 349.
(42) Spirlet, M.-R.; Rebizant, J.; Loncin, M.-F.; Desreux, J. F. *Inorg. Chem.* **1984**, *23*, 359.
(43) Maurya, M. R.; Zaluzec, E. J.; Pavkovic, S. F.; Herlinger, A. W. *Inorg. Chem.* **1991**, *30*, 3657.
(44) Bulach, V.; Mandon, D.; Fischer, J.; Weiss, R. *Inorg. Chim. Acta* **1993**, *210*, 7.

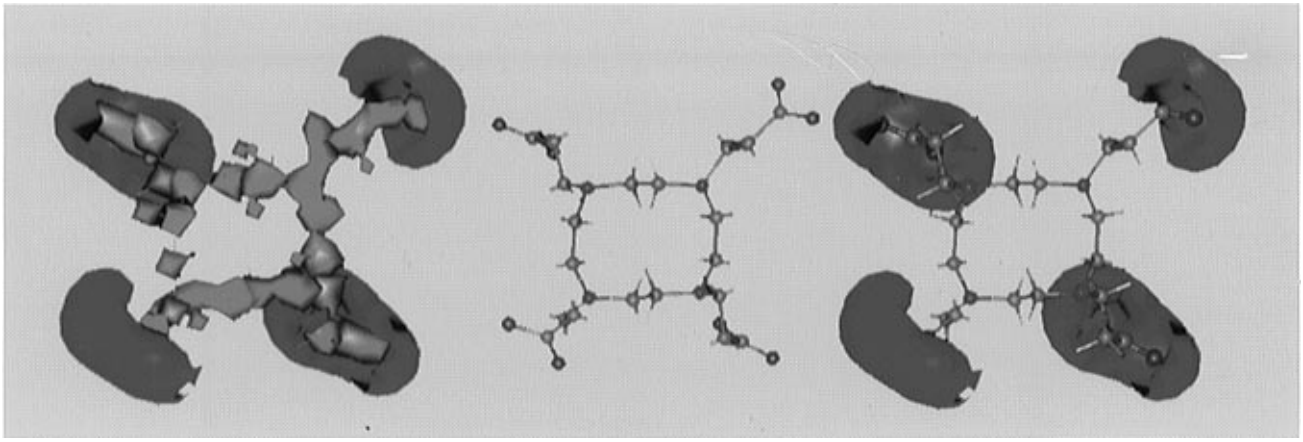

Figure 4. MEP and molecular structure of the DOTP ligand (same contours as Figure 3).

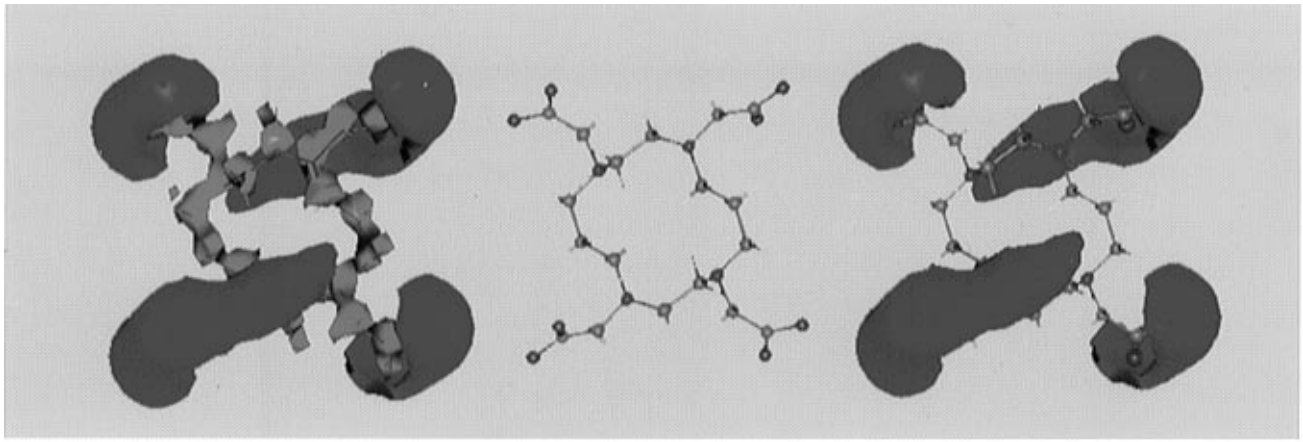

Figure 5. MEP and molecular structure of the TETA ligand (same contours as Figure 3).

nitrogen atoms are extended out of the cycle, whereas the two other functionalized chains are folded to form an intramolecular three-center hydrogen bond[45] between the HN1−N1 donor group and the O3 and N2 acceptors. The geometry of these intramolecular hydrogen bonds is given in Table 6. The sum of the three angles N1−HN1···O3, N1−HN1···N2, and O3···HN1···N2 is 360, 359, and 349° for **1**−**3**, respectively. In **1**, the extended propionate chains are in the four nitrogen atom mean plane; this is not the case in **2** and **3** where two adjacent propionate arms are located above the nitrogen atom mean plane, and the two others below, giving rise to a *trans*-IV configuration.[46]

In conclusion, we have then shown that at least two different coordination modes of the TETP ligand may occur with lanthanide ions. This is surprising because these metallic ions have similar chemical behavior. We can explain these results by molecular modeling.

Molecular Modeling. Gd/DOTA Complex. The experimental[41] conditions for obtaining the Gd/DOTA crystals imply the reaction of the completely deprotonated ligand $DOTA^{4-}$ with Gd^{3+}. A very simplistic picture of the Gd−DOTA complexation mechanism would be to neglect the solvent effects and focus only on the electrostatic part of the interaction. Indeed, it is well-known that the metal−ligand binding in alkaline earth and lanthanide complexes is predominantly electrostatic.[40] In this context the metallic cation would approach the electron-rich sites of the ligand. The calculated MEP's for DOTA show that negative surfaces are localized on the four carboxylate groups and on one side of the cycle cavity (Figure 3). As reported in other theoretical studies,[47,48] for the most stable configuration of cyclen (*trans*-I) all the 4 nitrogen lone pairs are oriented on one side of the cycle explaining the calculated negative MEP on this side. One can suppose that the metallic cation in the first step approaches from this side, coordinates the 4 nitrogen atoms, and then coordinates the four carboxylic arms. In order to test this hypothesis, the complexation process of Gd^{3+} with DOTA has been examined by molecular dynamics simulations (200 ps) using the ESFF empirical force field. The starting model consisted of Gd^{3+} located 10 Å from the center of the free ligand. The simulations carried out in vacuum showed two different mechanisms for the complexation of Gd^{3+} with DOTA. In the first mechanism the metallic cation is placed perpendicularly to the plane of the cyclic cavity, Gd^{3+} approaches the center of the cycle coordinating first the four N atoms, and then the arms slowly fold to coordinate the metallic center via the oxygen atoms. In the second case, Gd^{3+} is initially placed in the plane of the cycle, preliminary coordination being through one of the carboxylic arms. The four arms (the one coordinated to Gd^{3+} and three free ones) slowly fold resulting in Gd^{3+} coordinated to the four oxygen atoms of the four carboxylic groups, and in the last stage the cation coordinates to the nitrogen atoms of the cycle. As the solvent effects were neglected it is difficult on the basis of these simulations to discriminate between these two possible complexation mechanisms. Note that both mechanisms predict only

(45) Jeffrey, G. A.; Mitra, J. *Acta Crystallogr.* **1983**, *B39*, 469.
(46) Bosnich, B.; Poon, C. K.; Tobe, M. L. *Inorg. Chem.* **1965**, *4* (8), 1102.
(47) Thîm, V. J.; Fox, C. C.; Boyens, J. C. A.; Hancock, R. D. *J. Am. Chem. Soc.* **1984**, *106*, 5947.
(48) Adam, K. R.; Antolovich, M.; Brigden, L. G.; Lindoy, L. F. *J. Am. Chem. Soc.* **1991**, *113*, 3346.

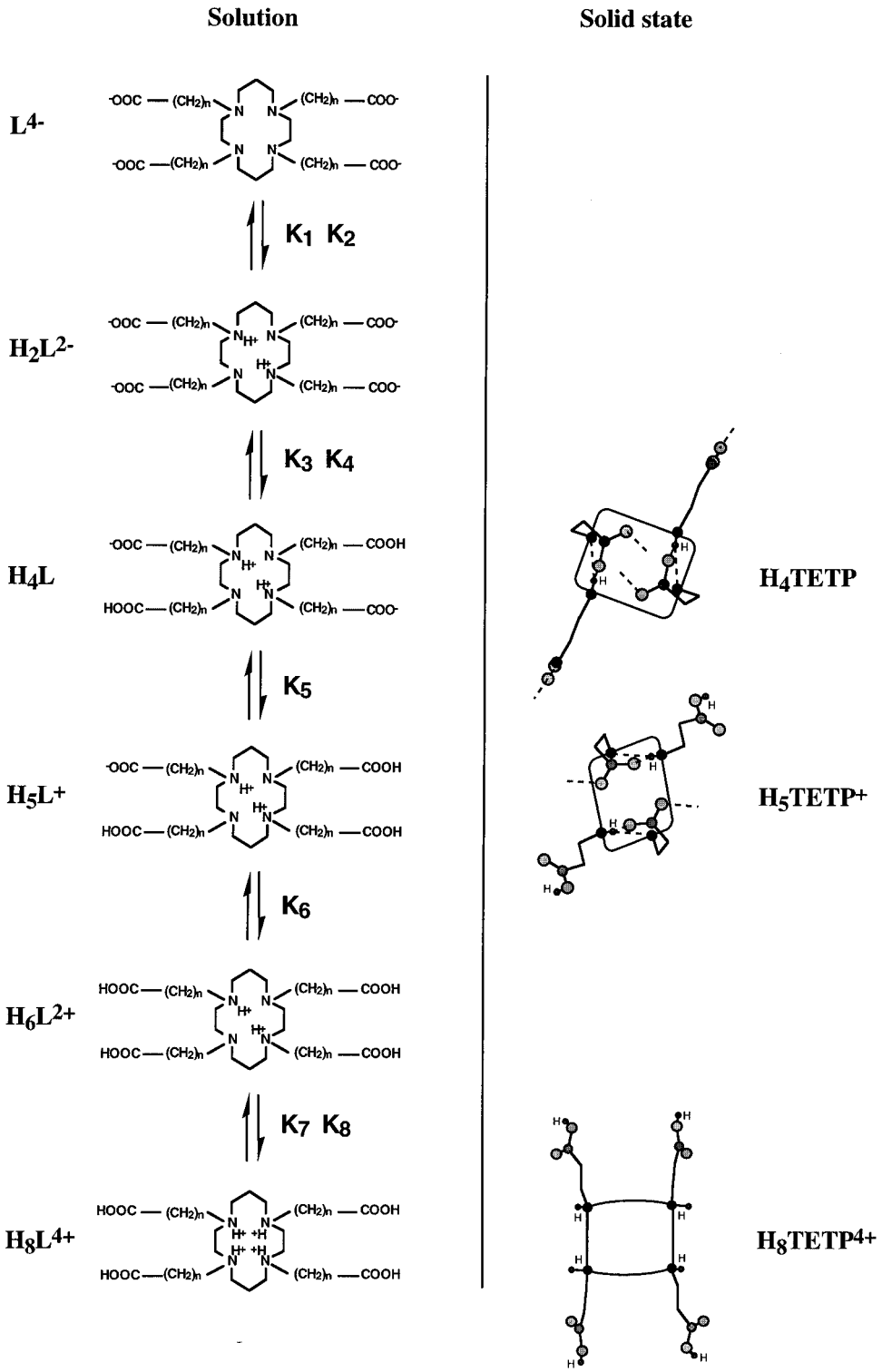

Figure 6. Protonation scheme of TETP.

one final structure in good agreement with the observed experimental one: The initial attack of the Gd^{3+} is observed in both cases toward sites of the ligand in which the MEP has minimum values. We will rely on this result to explain the coordination scheme of the newly formed complexes.

Gd/DOTP Complex. Influence of the Length of the Arm on the Coordinating Mode. The crystal structure of Gd/DOTP has not yet been determined. The coordination mode of this complex is only deduced from spectroscopic and analytical data. We have shown by fluorescence spectroscopy that the Gd/DOTA complex is more stable than Gd/DOTP. This observation suggests that the metallic cation in the later complex is certainly coordinated only through the oxygen atoms of the carboxylic groups. This assumption can be examined through the MEP topology of DOTP. As reported in Figure 4, DOTP does not exhibit a negative surface localized on the center of the cavity of the macrocycle. This is certainly related to the higher flexibility of the macrocyclic ligand due to the increase of the length of its substituent arms compared to DOTA, leading to a higher stability of the *trans*-III conformer where two nitrogen lone pairs are on one side of the cycle and the two others on the other side.

Gd/TETA Complex. Influence of the Size of the Macrocycle on the Coordination Mode. Fluorescence spectra of Gd/

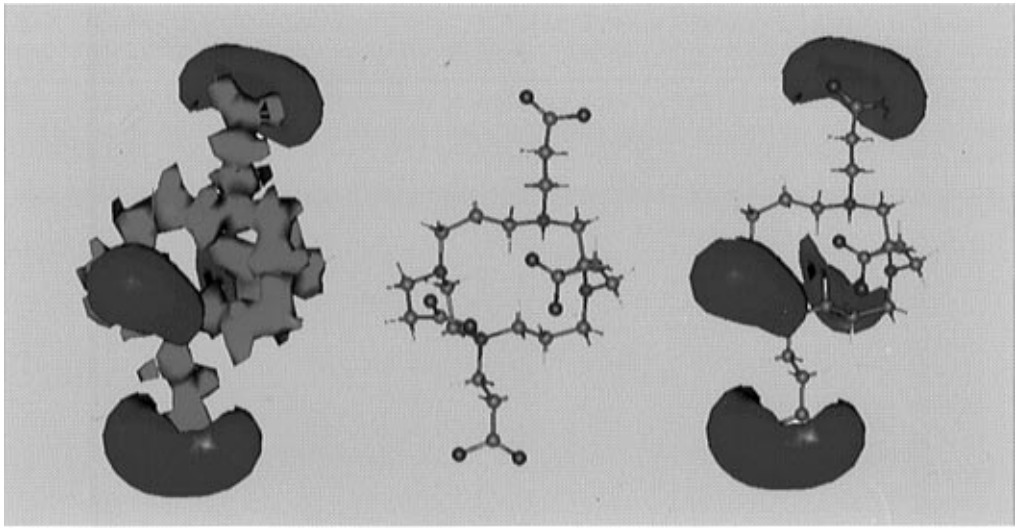

Figure 7. MEP and molecular structure of the H_2TETP ligand. (The contour level used to plot the MEP surfaces has been chosen at 0.15 au.).

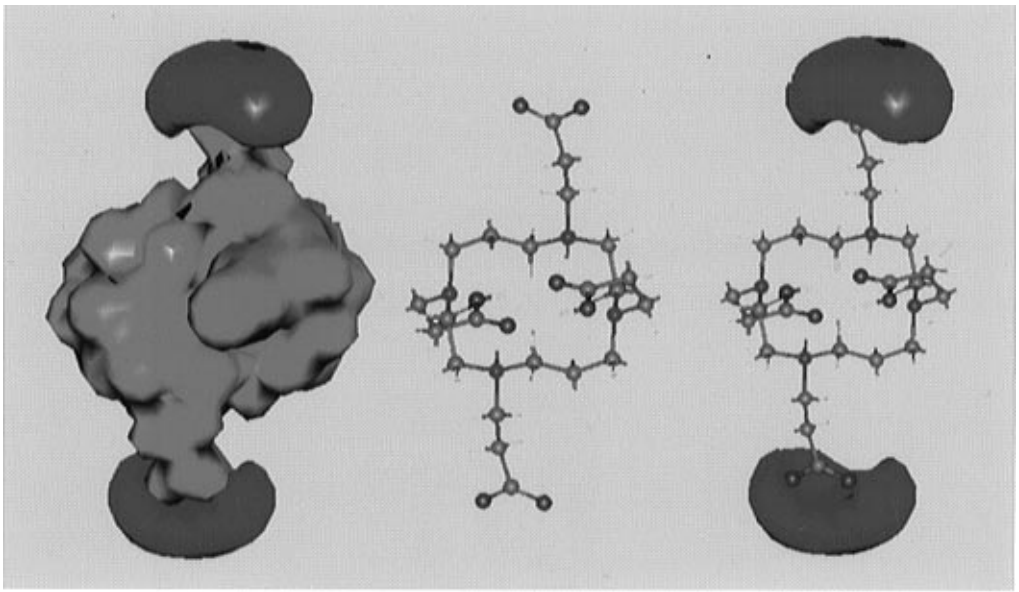

Figure 8. MEP and molecular structure of the H_4TETP ligand. (The contour level used to plot the MEP surfaces has been chosen at 0.075 au.).

TETA complexes indicate that the metallic cation is principally coordinated through the carboxylate arms of the ligand. However, this complex exhibits a metal to nitrogen band which is absent in Gd/DOTP. It is also worth noting that this absorption band is weaker than that observed for Gd/DOTA. Therefore, the Gd atom in Gd/TETA might not be coordinated to all nitrogen atoms of the cycle. In Figure 5, the MEP of TETA shows clearly the increased tendency for a cation to bind to the nitrogen atoms when moving from DOTP to TETA and to DOTA. The negative MEP surfaces on TETA reflects the positions of carboxylic groups and the conformation of the macrocycle. Hence, the more stable conformation for TETA is the *trans*-III, while it is the *trans*-I for DOTA. As reported in previous studies[47] the *trans*-I form for a 14-membered ring can easily be interconverted to *trans*-III one because of the slight difference in energy between them. This fact could explain why another coordination mode has been observed for the Tb/TETA complex.[40]

Ce/TETP, Gd/TETP, and Eu/TETP Complexes. Influence of the TETP Ligand Protonation Scheme on Its Coordination Mode. In Figure 6 we report the protonation scheme of the TETP ligand in the solid state.[49] As previously shown by the X-ray crystal structure studies of the tetra-, penta-, and octaprotonated forms of TETP,[38] first, two nitrogen atoms in *trans* position are protonated giving rise to the H_2TETP diprotonated form of the ligand. The H_4TETP tetraprotonated form corresponds to a half-protonation of each carboxyl group of the ligand, each carboxyl group sharing its hydrogen atom with another COO^- group of another TETP macrocycle. The penta- and hexaprotonated forms involve the total protonation of the carboxyl groups of the side chains bound to the protonated and nonprotonated nitrogen atoms, respectively. Finally, the octaprotonated form corresponds to the protonation of the two remaining nitrogen atoms. It is evident that the H_4TETP neutral form, as observed through X-ray crystallography, cannot exist in solution: More certainly, in this case, either the carboxyl arms bound to the protonated nitrogen atoms or those bound to the nonprotonated nitrogen atoms must be protonated. This

(49) Dahaoui-Gindrey V. Ph.D. Thesis, Université Henri Poincaré, Nancy 1, 1995.
(50) Baes, C. F., Jr.; Mesmer, R. E. *The hydrolysis of Cations*; Wiley: New York, 1976.

Table 7. Protonation Constants of the TETP and TETA Macrocycles

macrocycle	pK_1	pK_2	pK_3	pK_4	pK_5	pK_6
TETP	10.47(3)	10.65(2)	4.33(2)	3.60(3)	3.06(4)	2.28(4)
TETA	11.24(1)	9.87(1)	4.25(1)	3.50(1)	2.17	1.42

second option is more favorable, because the electrostatic repulsion between the negative charges is lower.

As discussed above, the crystal structures of Ce/TETP and Gd(Eu)/TETP present different coordination modes. The chemical behavior of the lanthanide cations is similar and cannot explain these experimental observations. The only parameter which was different in the respective complexation reactions of Ce and Gd (Eu) reactions with the TETP ligand was the pH of the solution. As pointed out in the Experimental Section, the metalation reaction was carried out in buffered solutions for the Gd and Eu complexes (pH = 3.5/3.8), while it was performed in water solution for the Ce complex (pH = 3.2). Moreover, it is well-known that aqueous solutions of lanthanide cations undergo hydrolysis reactions above pH 5 leading thus to $[Ln(OH)_n]^{3-n}$ species implying a lowering of the pH. The pH lowering below the value 3.60 (Table 7) implies the protonation of TETP to H_4TETP (tetraprotonated form), while in the buffered case the ligand corresponds to the H_2TETP diprotonated one. Consequently, two distinct protonated forms of the ligand have been generated during the complexation reactions: H_2TETP and H_4TETP corresponding to the metalation reactions by Gd (Eu) and Ce, respectively. The calculated MEP for these two forms reported in Figures 7 and 8 clearly shows that all the carboxylic groups of the H_2TETP may bind a lanthanide ion, whereas only the two extended arms of H_4TETP may bind the cation. These results are in excellent agreement with the coordination mode observed in the solid state (X-ray crystalline structures). However some differences can be noted: Complexation of Ce with H_4TETP leads to Ce/H_2TETP, and complexation of Gd(Eu) with H_2TETP results in Gd(Eu)/H_3TETP. The pH of the solutions (buffer and unbuffered) changes continuously as the complexation reaction progresses. Indeed in the case of Ce−H_4TETP complexation, the monitored pH during complex formation changes from 3.2 (H_4TETP being the majority form) at the beginning of the reaction to 4.4 (H_2TETP being the majority form) at the end of the reaction (Table 7). The MEP maps of H_4TETP indicate that the ligand must be initially attacked by the metal at the extended carboxylic arm sites (Figure 8). The pH equilibrium moves toward greater values of pH as the metal cations coordinate to the ligand leading to the Ce/H_2TETP form of the complex (Table 7). This behavior is due to the well-known drawback of this class of macrocyclic ligands characterized by their slow rate of complexation compared to the hydrolysis reactions of lanthanide cations.

Conclusion

In the present work we have reported a combined crystallographic and theoretical study of the metal-to-ligand coordination in the *N*-propionate (acetate)-substituted tetraazamacrocycle series. Using this approach, we have been able to understand and even to predict the coordination scheme for this class of ligands. The crystal data have been of fundamental importance to carry out this study. Indeed, due to the high flexibility of the ligands, the crystallographic parameters are necessary to make a selection between the numerous possible conformers. Preliminary molecular mechanics calculations combined with crystal data results have been used to determine the most probable conformer for which a single DFT calculation has been performed to define the MEP topography. The MEP has thus been used for interpreting and predicting the reactive behavior of electrophilic reactions between metallic cations and macrocyclic ligands.

This study clearly shows that three major factors have to be considered in order to explain the reactivity of this class of ligands toward metallic ions. These factors are as follows:

(i) The length of the N-appended substituent arms is important; in the cyclen series short arms (acetate) favor a 4N/4O coordination scheme, while with long ones (propionate) the metal is coordinated only to the oxygen atoms.

(ii) The size of the cavity of the macrocycle must also be considered. Its effect is clearly observed when comparing metal coordination with DOTA and TETA ligands; the Gd, Eu, and Ce/TETA complexes as studied by fluorescence spectroscopy[51] present mainly metal ion coordination through the oxygen atoms of the carboxylate groups, contrary to the well-known 4N/4O coordination observed for DOTA.

(iii) To our knowledge this study shows for the first time that the coordination scheme for this class of ligand is critically dependent on the pH of the metalation reaction. In this work we have shown that the metalation of the H_2TETP involves the four carboxylate arms, while only two of them participate in metal ion coordination for the tetraprotonated H_4TETP form. Very recent results[52] confirm the role of the degree of protonation of the ligand in the coordination scheme: We just solved the X-ray structure of Ce/H_2TETP synthesized in the same pH conditions as the Gd and Eu complexes; in this new structure, the Ce ion exhibits the same coordination polyhedron as in the Gd and Eu complexes. It should also be noted that the Ce ion exhibits a +III oxidation state as clearly shown by the X-ray crystal structure determination.

Acknowledgment. We thank the CNRS and both our Universities ("Université Henri Poincaré" and "Université de Bourgogne") for supporting this study.

Supporting Information Available: Tables of anisotropic thermal motion parameters, positional parameters for hydrogen atoms, and least-squares planes for the Ce/TETP (**1**), Gd/TETP (**2**), and Eu/TETP (**3**) complexes (9 pages). Ordering information is given on any current masthead page.

IC960934H

(51) Lemeune, S.; Barbette F.; Pullumbi P.; Guilard R. To be published.
(52) Dahaoui-Gindrey V.; Barbette F.; Pullumbi, P.; Lecomte, C.; Guilard, R. To be published.